Complex Systems **7** (1993) 367–388

Monomial Cellular Automata

Ron Bartlett*
Max Garzon†
Department of Mathematical Sciences,
The University of Memphis,
Memphis, Tennessee 38152, USA

Abstract. We investigate the dynamics of monomial cellular automata, whose next-state is given as a product of the neighboring states. Monomial cellular automata provide a multiplicative analogue of additive cellular automata with novel dynamical features. Phase portraits are given for monomials of degree two and three, along with general methods to obtain them. Monomials of higher degree are analyzed via a superposition principle.

1. Introduction

Linear or additive cellular automata (CAs) have remained, since their early inception, the most amenable to rigorous analytic treatment [1, 2, 3] due to the *superposition principle*. Recently, Reimen [4] extended the superposition principle to CAs over commutative monoids. With the binary operation given by juxtaposition, the superposition principle is then given by

$$T(xy) = T(x)T(y) \tag{1}$$

where T is the global dynamics and x and y are *configurations* consisting of bi-infinite words over a finite set of states Q, that is,

$$x = \ldots x_{-2}x_{-1}x_o x_1 x_2 \ldots \qquad x_i \in Q$$

and the binary operation is applied pointwise, that is,

$$(xy)_i = x_i y_i.$$

Substituting for both sides of equation (1) gives

$$(x_i y_i)(x_{i+1}y_{i+1}) = (x_i x_{i+1})(y_i y_{i+1}).$$

*Electronic mail address: bartlettr@hermes.msci.memst.edu
†Electronic mail address: garzonm@hermes.msci.memst.edu

Therefore,

$$\forall a, b, c, d, \quad (ab)(cd) = (ac)(bd).$$

As Reimen pointed out, this condition is satisfied by a *commutative monoid*: examples include $\langle \mathbf{Z}_m, \bullet \rangle$, the residue classes of integers modulo m under multiplication.

Indeed, a multiplicative version of the superposition principle provides a direct approach to analyze CAs over $\langle \mathbf{Z}_m, \bullet \rangle$, whose local rule is given by a *product* of the neighboring states

$$\delta_{\text{mono}}(\vec{x}) \equiv \prod_{j=1}^{n} x_{i+j}^{p_j} \pmod{m},$$

where $\vec{x}_i$ is the *ordered* neighborhood vector $(x_i, \ldots, x_{i+n-1})$ of cell i. We refer to these as *monomial* cellular automata because they are a particular case of a more general class of CAs whose local rules can be expressed as *polynomials*, that is, as sums of S monomial terms with coefficients a_k:

$$\delta_{\text{poly}}(\vec{x}) \equiv \sum_{k=1}^{S} a_k \left(\prod_{j=1}^{n} x_j^{p_j} \right) \pmod{m}.$$

Hedlund [5] has shown that any CA over a prime number of states p can be expressed as a polynomial of degree less than p, where the degree of the polynomial is given by $\max(p_j)$. We then associate the *complexity* of a CA with the *degree* of the polynomial $P(x_1 \ldots x_n) = \delta_{\text{poly}}(\vec{x})$. The lowest degree CAs are those with linear (additive) rules such that $\max(p_j) = 1$. The degree of a monomial term $\prod_{j=1}^{n} x_j^{p_j}$ is the number of variables x_j with nonzero exponents p_j (we assume $x_j^0 = 1$). Thus, linear (additive) CAs consist of sums of monomials of degree 1, whereas bilinear (quadric) CAs consist of sums of monomials of degree 2, and so on.

1.1 Relation to linear CAs

Monomial CAs are the multiplicative analogues of additive (linear) CAs. The trajectories of single pixels are described by rows of Pascal's triangle modulo k. For example, consider the orbit of $\overline{1}$ under

$$\pi_{1,1}(x)_i \equiv x_{i-1} x_{i+1} \pmod{m} \tag{2}$$

below.

$$\begin{array}{c}
\ldots 11111\underline{s}11111\ldots \\
\ldots 1111s\underline{1}s1111\ldots \\
\ldots 111s1\underline{s}^2 1s111\ldots \\
\ldots 11s1s^3\underline{1}s^3 1s11\ldots \\
\ldots 1s1s^4 1\underline{s}^6 1s^4 1s1\ldots \\
\vdots
\end{array}$$

The underscore $\underline{s}$ indicates the center cell. Here the exponents of s are the binomial coefficients. The following definition is taken from Aho and Honda [2].

$$\begin{array}{ccccc} & & \delta_\Pi & & \\ & \mathcal{C} & \longrightarrow & \mathcal{C} & \\ \log_g & \downarrow & & \downarrow & \log_g \\ & \mathcal{C} & \longrightarrow & \mathcal{C} & \\ & & \delta_\Sigma & & \end{array}$$

Figure 1: Conjugacy between linear and monomial CAs over $\langle \mathbf{Z}_p, +, \bullet \rangle$.

Definition 1.1. *A state s is* quasi-idempotent *if there exist $d, k \in \mathbf{Z}^+$ such that $s^{d+k} = s^d$, where the least such d is called the* idempotent degree *of s and k is called the* idempotent order *of s, denoted $ord(s)$.*

Now if $s^{d+k} = s^d$ for some integer $k > 0$, then the exponents repeat modulo k where $k = \mathrm{ord}(s)$. These patterns are well understood for prime k ([6]; see also [7] and [8]), but not for composite k. For the monomial of degree 2 given by equation (2), if k is a power of 2, the orbit of $\overline{1} = \ldots 111 \ldots$ will converge to a limit cycle, otherwise it will diverge. Since a *unit* (invertible element) cannot be idempotent, all finite perturbations of $\overline{1}$ by units have divergent orbits. In particular, only the orbits of finite perturbations of $\overline{1}$ by zero divisors can converge.

For prime p, $\langle \mathbf{Z}_p, +, \bullet \rangle$ is a field that contains only one *non-unit*, 0. Therefore, only configurations containing a 0 can lead to convergent orbits. For m with primitive roots, $\langle \mathbf{Z}_m^*, \bullet \rangle \cong \langle \mathbf{Z}_{\phi(m)}, + \rangle$, where $\phi(m)$ is Euler's ϕ-function and $\langle \mathbf{Z}_m^*, \bullet \rangle$ is the set of units modulo m (those *coprime* to m). If g is a primitive root of m, $\langle \mathbf{Z}_m^*, \bullet \rangle$ is a *cyclic* group generated by g. In this case the *discrete logarithm* $\log_g$ given by

$$\delta_\Sigma(\vec{x}) \equiv \log_g(\delta_\Pi) \equiv \log_g \left(\prod_i x_j^{p_j} \pmod m \right) \tag{3}$$

$$\equiv \sum_j p_j \log_g x_j \pmod{\phi(m)} \tag{4}$$

provides a *topological conjugacy* between a monomial CA over $\langle \mathbf{Z}_m^*, \bullet \rangle$ and a linear CA over $\langle \mathbf{Z}_{\phi(m)}, + \rangle$, ($\log_g$ is locally defined, hence it is continuous and surjective). If $\mathcal{C}$ denotes the *configuration space* consisting of the set of configurations endowed with the product topology, then the diagram in Figure 1 commutes.

It is well known that the integers

$$1, 2, 4, p^\alpha, 2p^\alpha$$

have primitive roots where p is any odd prime (see [9, Theorem 4.11]).

In the general case, $\log_g$ provides an isomorphic copy of a linear rule over the units only. It is also necessary to examine the behavior over the zero divisors.

1.2 Relation to Wolfram classes

The CA classification scheme proposed by Wolfram [11] and refined by Culik and Yu [10] (for which the general problem of classification is undecidable) provides another approach to studying monomial CAs. Here we briefly review this scheme as given by Culik and Yu [10].

In what follows, a *stable state* s is one that is invariant under iteration of the local rule, that is, $\delta(s \dots s) = s$. A *homogenous* (bi-infinite) configuration of s, denoted $\overline{s}$, is one in which every cell is in state s. A *finite s-configuration* is one in which all but finitely many cells are in state s. The stable state for an additive CA over $\langle \mathbf{Z}_m, + \rangle$ is 0, and the corresponding *homogenous* configuration is $\overline{0}$. The notation $\underline{s}$ identifies s as the cell at the origin. For a multiplicative CA over $\langle \mathbf{Z}_m, \bullet \rangle$ the stable state is 1 and the homogenous configuration is $\overline{1}$.

Definition 1.2. (Wolfram Classes as refined by Culik and Yu [10].)

Class I *(Black Hole): All finite s-configurations evolve to the homogeneous configuration of s.*

Class II *(Periodic Orbits): All finite s-configurations have an eventually periodic evolution.*

Class III *(Chaotic Orbits): it is decidable whether c_1 evolves to c_2 for arbitrary finite s-configurations c_1 and c_2.*

Class IV *(Universal): All cellular automata.*

Note that Class I $\subset$ Class II $\subset$ Class III $\subset$ Class IV.

Following this scheme, we investigate the dynamics of monomial CAs by examining the evolution of finite 1-configurations, which we refer to as *perturbations* of $\overline{1}$. We show that monomial CAs only belong to Classes I, II, and III.

For CAs, limit cycles correspond to periodic configurations. We describe a periodic configuration by a pattern. For example, we denote the pattern $\dots 010101 \dots$ by $\overline{01}$. Note that we do not distinguish an *origin*, as in $\dots 01\underline{0}101 \dots$. A *pattern* is the *equivalence class* of periodic configurations modulo a shift. For monomial CAs, this is the same as considering equivalent classes of limit cycles modulo the cycle length, or period. For example, we will consider the 2-cycle $\dots 01\underline{0}10 \dots \leftrightarrow \dots 10\underline{1}01 \dots$ to be in the same class as the fixed points $\dots 01\underline{0}10 \dots$ and $\dots 10\underline{1}01 \dots$. This is because all the patterns in the basic block of a limit cycle must have the same number of 0s, as we shall explain.

The structure of this paper is as follows. In section 2 we examine the monomials of degree 2 over $\mathbf{Z_2}$. In section 3 we investigate monomials of degree 3 over $\mathbf{Z_2}$. In section 4 we consider higher dimensional analogues of the monomials in previous sections. In section 5 we consider the effects of extending the state sets, that is, for monomials over $\mathbf{Z_m}$.

$$
\begin{array}{c}
\ldots 1111111\underline{0}1111111\ldots \\
\ldots 1111110\underline{1}0111111\ldots \\
\ldots 1111101\underline{0}1011111\ldots \\
\ldots 1111010\underline{1}0101111\ldots \\
\ldots 1110101\underline{0}1010111\ldots \\
\ldots 1101010\underline{1}0101011\ldots \\
\vdots \\
\ldots 1010101\underline{0}1010101\ldots \\
\ldots 0101010\underline{1}0101010\ldots
\end{array}
$$

Figure 2: Perturbation of $\overline{1}$ under $\pi_{1,1}(x)_i \equiv x_{i-1}x_{i+1} \pmod 2$.

2. Monomials of degree two

We begin by examining monomial CAs in dimension one by distinguishing two subcases:

1. the *symmetric* monomials, given by

$$\pi_{r,r}(x)_i \equiv x_{i-r}x_{i+r} \pmod m$$

2. the *asymmetric* monomials, given by

$$\pi_{r,k}(x)_i \equiv x_{i-r}x_{i+k} \pmod m$$

where $r > k$ (neighborhood of radius r).

2.1 Symmetric monomials of degree two

We begin with a typical example. Consider the monomial, given by

$$\pi_{1,1}(x)_i \equiv x_{i-1}x_{i+1} \pmod 2.$$

First note that $\overline{0}$ is a fixed-point attractor, as any perturbation (replacing a finite number of 0s with 1s) leads back to $\overline{0}$. In contrast, $\overline{1}$ is a fixed-point repellor, as any perturbation (replacing a finite number of 1s with 0s) never leads back to $\overline{1}$. Note further that any perturbation of the center neighborhood of $\overline{1}$ is propagated left and right into adjacent neighborhoods. We call this *idempotent propagation (idemprop)*. For example, consider the simplest perturbation of $\overline{1}$ under $\pi_{1,1}$ in Figure 2.

The limit cycle is a 2-cycle given by $\overline{01} \leftrightarrow \overline{10}$. Other *perturbations* of $\overline{1}$ consist of injecting a finite number of 0s. Given *idemprop*, we envision two *waves* of 0s meeting in or out of phase. For example, perturbing $\overline{1}$ with a pair of 0s, separated by an *odd* block of 1s, also yields an orbit converging to the 2-cycle $\overline{01} \leftrightarrow \overline{10}$:

$$\pi^t_{1,1}(\overline{1}01^{2l+1}0\overline{1}) = \pi^t_{1,1}(\ldots 110\overbrace{1\ldots 1}^{2l+1}011\ldots) \longrightarrow \overline{01} \leftrightarrow \overline{10}$$

$$
\begin{array}{c}
\ldots 1111111011\underline{1}1101111111\ldots \\
\ldots 1111110101\underline{1}1010111111\ldots \\
\ldots 1111101010\underline{1}0101011111\ldots \\
\ldots 1111010101\underline{0}1010101111\ldots \\
\ldots 1110101010\underline{1}0101010111\ldots \\
\ldots 1101010101\underline{0}1010101011\ldots \\
\vdots \\
\ldots 1010101010\underline{1}0101010101\ldots \\
\ldots 0101010101\underline{0}1010101010\ldots
\end{array}
$$

Figure 3: Superimposing waves for $\pi_{1,1}(x)_i \equiv x_{i-1}x_{i+1} \pmod 2$.

$$
\begin{array}{c}
\ldots 1111111011\underline{1}1101111111\ldots \\
\ldots 1111110101\underline{1}1010111111\ldots \\
\ldots 1111101010\underline{0}0101011111\ldots \\
\ldots 1111010000\underline{0}0010101111\ldots \\
\ldots 1110100000\underline{0}0001010111\ldots \\
\ldots 1101000000\underline{0}0000101011\ldots \\
\vdots \\
\ldots 0000000000000000000\ldots
\end{array}
$$

Figure 4: Annihilating waves for $\pi_{1,1}(x)_i \equiv x_{i-1}x_{i+1} \pmod 2$.

We say that the waves are *superimposing* (see Figure 3).

In contrast, perturbing $\overline{1}$ with a pair of 0s, separated by an *even* block of 1s, yields an orbit converging to the attractor $\overline{0}$, that is,

$$\pi^t_{1,1}(\overline{1}01^{2l}0\overline{1}) = \pi^t_{1,1}(\ldots 110\overbrace{1\ldots 1}^{2l}011\ldots) \longrightarrow \overline{0}$$

We say that the waves are *annihilating* (see Figure 4).

Having considered all possible perturbations of $\overline{1}$, we turn next to perturbations of the 2-cycle $\underline{0}\overline{1} \leftrightarrow \underline{1}\overline{0}$. Perturbing this 2-cycle by replacing a 0 with a 1 returns the 2-cycle.

$$\pi^t_{1,1}(\overline{01}\underline{1}\overline{10}) = \pi^t_{1,1}(\ldots 0101\underline{1}1010\ldots) \longrightarrow \underline{0}\overline{1} \leftrightarrow \underline{1}\overline{0}$$

Perturbing the 2-cycle by replacing a 1 with a 0 gives rise to an orbit converging to $\overline{0}$.

$$\pi^t_{1,1}(\overline{10}\underline{0}\overline{01}) = \pi^t_{1,1}(\ldots 1010\underline{0}0101\ldots) \longrightarrow \overline{0}$$

The 2-cycle $\underline{0}\overline{1} \leftrightarrow \underline{1}\overline{0}$ is a *saddle* pattern, in the sense that it *attracts* some nearby patterns (perturbations) yet *repels* others.

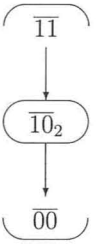

Figure 5: Phase portrait for $\pi_{1,1}(x)_i \equiv x_{i-1}x_{i+1} \pmod 2$.

$$
\begin{array}{c}
\ldots 111^{r-1}11^{r-1}\underline{0}1^{r-1}11^{r-1}11\ldots \\
\ldots 111^{r-1}01^{r-1}\underline{1}1^{r-1}01^{r-1}11\ldots \\
\ldots 101^{r-1}11^{r-1}\underline{0}1^{r-1}11^{r-1}01\ldots \\
\ldots 111^{r-1}01^{r-1}\underline{1}1^{r-1}01^{r-1}11\ldots \\
\vdots \\
\ldots 101^{r-1}11^{r-1}\underline{0}1^{r-1}11^{r-1}01\ldots \\
\ldots 111^{r-1}01^{r-1}\underline{1}1^{r-1}01^{r-1}11\ldots
\end{array}
$$

Figure 6: Perturbation of $\overline{1}$ under $\pi_{r,r}(x)_i \equiv x_{i-r}x_{i+r} \pmod 2$.

The phase portrait is given in Figure 5. To simplify the diagrams, we have followed several conventions. First, as mentioned in the introduction, we give only one of the patterns in a limit cycle, and indicate the length of the cycle by a subscript. For example, the 2-cycle $\overline{01} \leftrightarrow \overline{10}$ is denoted $\overline{01}_2$. Second, patterns are arranged so that they can be reached by a perturbation of patterns in a level above. The patterns in consecutive levels in the diagram differ in the number of 0s, by a single 0. The basin of attraction of $\overline{0}$ is nearly the entire configuration space, that is, $\pi_{1,1}^t(x) \to \overline{0}$ almost everywhere.

Next we analyze the dynamics of the symmetric monomial given by

$$\pi_{r,r}(x)_i \equiv x_{i-r}x_{i+r} \pmod 2$$

Consider the orbit of the slightest perturbation of $\overline{1}$ in Figure 6. The limit cycle is given by the pair of bi-infinite *patterns* $\overline{01^{r-1}\underline{1}1^{r-1}} \leftrightarrow \overline{11^{r-1}\underline{0}1^{r-1}}$. Again, it is easy to see that $\overline{0}$ is a fixed-point attractor, while $\overline{1}$ is a fixed-point repellor.

Due to *idemprop*, the perturbations of $\overline{1}$ that are contained in a single block of size $n-1 = 2r$ (neither all 1s, nor all 0s) are all *gardens of Eden*. There are at most 2^{n-1} distinct blocks $b_1 \ldots b_{n-1}$, each of which tends to a limit cycle pattern $\overline{b_1 \ldots b_{n-1}}$. These blocks then constitute a sufficient set of perturbations of $\overline{1}$ to produce all the limit cycles. Of course, a given limit cycle may contain more than one pattern.

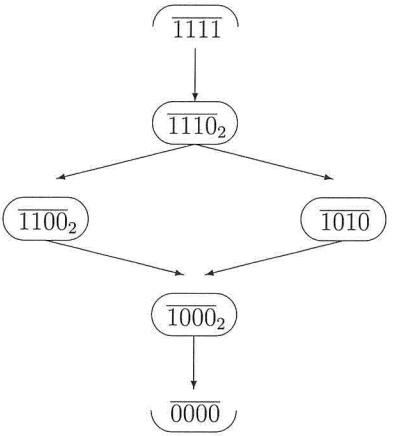

Figure 7: Phase portrait for $\pi_{2,2}(x)_i \equiv x_{i-2}x_{i+2} \pmod 2$.

Next, we perturb each of the patterns in each limit cycle in order to determine their asymptotic behavior. This is easily accomplished, as changing a 1 to a 0 in any pattern leads to a pattern with fewer 1s, while changing a 0 to a 1 in any pattern returns the pattern. So each limit cycle is a *saddle* cycle, except the attractor $\overline{0}$ and the repellor $\overline{1}$. Also, each set of patterns constituting a limit cycle must have the same number of 0s. Hence, we have a partial ordering on the limit cycles, determined by the number of 0s in any one of their constituent patterns.

The global dynamics of the rule acts as a *gravitational field*, originating at $\overline{0}$ and pulling every configuration under the rule's evolution from $\overline{1}$ down to $\overline{0}$. We summarize these observations in the following.

Proposition 2.1. (The dynamics of $\pi_{r,r}(x)_i \equiv x_{i-r}x_{i+r} \pmod 2$.)
If $n = 2r + 1$, then

1. *There are at most 2^{n-1} limit cycles, each given by a distinct pattern, of the form $\overline{b_1 \dots b_{n-1}}$. Each is a saddle cycle, except the repellor $\overline{1}$ and the attractor $\overline{0}$.*
2. *The basin of attraction of $\overline{0}$ properly contains the set of configurations with at least one block of 0^{n-1}.*

In Figure 7, we give the phase portrait for $r = 2$. The patterns may have more than one representation. For example $\overline{1110} = \overline{0111} = \overline{1011} = \overline{1101}$. Any given pattern can be reached by a perturbation of a pattern above it in the diagram, and $x \to \overline{0000}$ almost everywhere.

In Figure 8, in order to gain an idea of the sequence of portraits for increasing r, we present the phase portrait for $r = 3$ as well. Recall there are

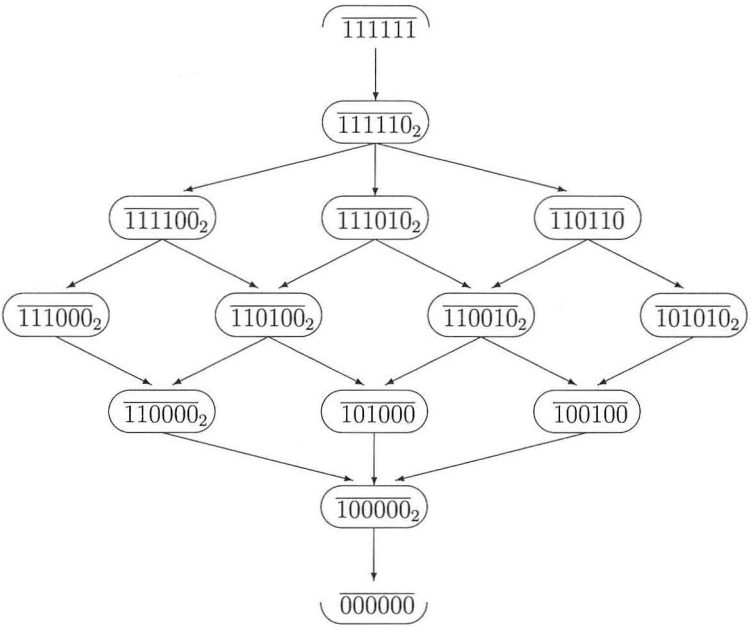

Figure 8: Phase portrait for $\pi_{3,3}(x)_i \equiv x_{i-3}x_{i+3} \pmod 2$.

paths in the diagram between higher and lower patterns where the arrows are not written in.

In the general case, the mixture of limit cycles depends on certain properties of r. For example, as r changes, the orbits of the *alternating* configuration $\overline{0011} = \ldots 00110011 \ldots$ are

$$\begin{aligned}
&\pi^t_{r,r}(\overline{0011}) \to \overline{0011}_2 \qquad r = 2, 3, 6, 7, 10, 11, \ldots \\
&\pi^t_{r,r}(\overline{0011}) \to \overline{0011} \qquad r = 4, 8, 12, \ldots \\
&\pi^t_{r,r}(\overline{0011}) \to \overline{0000} \qquad r = 1, 5, 9, 13, \ldots
\end{aligned}$$

Next we consider the asymmetric case.

2.2 Asymmetric monomials of degree two

First notice that an asymmetric monomial of degree 2 is equivalent to a *one-sided* monomial of degree 2 composed with a shift:

$$\pi_{r,k}(x)_i \equiv x_{i-r}x_{i+k} \pmod 2 = \sigma^k(\pi_{r+k,0}(x))_i$$

where $\sigma^k(x)_i = x_{i+k}$ is the left-shift applied k times. We begin then by examining the case where $k = 0$.

Consider the smallest perturbation of $\overline{1}$ in Figure 9. In general, there are 2^r distinct basic blocks $b_1 b_2 \ldots b_r$, each of which tends to a distinct fixed

$$\begin{array}{l}
\ldots 111\underline{1}01^{r-1}111\ldots \\
\ldots 111\underline{1}01^{r-1}01^{r-1}111\ldots \\
\ldots 111\underline{1}01^{r-1}01^{r-1}01^{r-1}111\ldots \\
\qquad\vdots \\
\ldots 111\underline{1}01^{r-1}01^{r-1}01^{r-1}01^{r-1}\ldots
\end{array}$$

Figure 9: Perturbation of $\overline{1}$ under $\pi_{r,k}(x)_i \equiv x_{i-r}x_{i+k} \pmod 2$.

point. Since we may pick any cell as the cell with the left-most 0, denoted $\underline{0}$, there are countably many fixed points for each distinct block. We summarize these observations as follows.

Proposition 2.2. (The dynamics of $\pi_{r,0}(x)_i \equiv x_{i-r}x_i \pmod 2$.)

1. *There are countably many fixed points in each of the 2^r distinct right-periodic patterns of the form $\overline{1\, b_1 \ldots b_r}$. Each is a saddle point, except the repellor $\overline{1}$ and the attractor $\overline{0}$.*
2. *The basin of attraction of $\overline{0}$ consists of the set of configurations of the form $\overline{0}1b_{i+1}b_{i+2}\ldots$, where the position of the leftmost 1 is arbitrary.*

The phase portrait for this case is well described by the proposition, so we omit a diagram.

Next we investigate the shifted dynamics of

$$\pi_{r,k}(x)_i \equiv x_{i-r}x_{i+k} \pmod 2 = \sigma^k(\pi_{r+k,0}(x))_i$$

where $r > k > 0$. The dynamics are two-sided, so there are no longer countably many limit cycles for each of the 2^n $(n = r + k)$ patterns, but at most one for each pattern. In general, each pattern represents a unique cycle of length $n = r + k$. However, patterns containing a subpattern may lead to a shorter cycle of length of the subpattern. We summarize these observations as follows.

Proposition 2.3. (The dynamics of $\pi_{r,k}(x)_i \equiv x_{i-r}x_{i+k} \pmod 2$.) *If $n = r + k$, then*

1. *There are at most 2^n limit cycles, each given by a distinct pattern of the form $\overline{b_1 b_2 \ldots b_n}$. Each is a saddle cycle, except for the repellor $\overline{1}$ and the attractor $\overline{0}$.*
2. *The basin of attraction of $\overline{0}$ properly contains those configurations with a block of 0^n.*

All the phase portraits consist of the pattern $\overline{01}$, as either a fixed point or a 2-cycle. The rest of the patterns consist of p-cycles, where p divides n. The

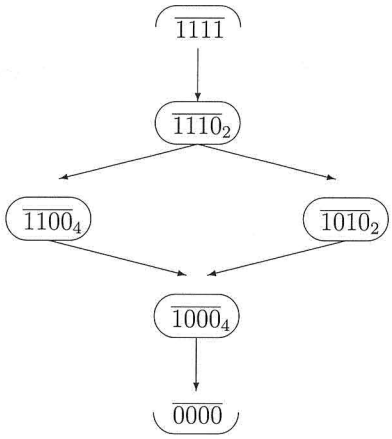

Figure 10: Phase portrait for $\pi_{1,3}(x)_i \equiv x_{i-1}x_{i+3} \pmod 2$.

phase portrait for $r = 1$ and $k = 3$ is given in Figure 10. Note the similarity with the symmetric case $r = 2$ in Figure 7.

When $r = 4$ and $k = 2$, $\overline{01}$ is a fixed point, and the rest of the phase portrait consists of only 3-cycles. We omit the diagram in the interest of space.

3. Monomials of degree three

In this section we examine monomials of degree 3 whose global dynamics in one dimension are given by

$$\pi_{r,j,k}(x)_i \equiv x_{i-r}x_{i-j}x_{i+k} \pmod m$$

Again, we distinguish between two subcases: the symmetric case where $r = k$ and $j = 0$, and the asymmetric case where $r \geq k > j > 0$. We begin with the symmetric case.

3.1 Symmetric monomials of degree three

Consider the symmetric monomial of degree 3 given by

$$\pi_{r,0,r}(x)_i \equiv x_{i-r}x_ix_{i+r} \pmod 2$$

This is just the two-sided analogue of $\pi_{r,0}(x)_i \equiv x_{i-r}x_i \pmod 2$ summarized in Proposition 2.2. A canonical example is the doubly infinite pattern $\overline{01^{r-1}}$ in Figure 11. Thus we have the following.

Proposition 3.1. (The dynamics of $\pi_{r,0,r}(x)_i = x_{i-r}x_ix_{i+r} \pmod 2$.)

$$\begin{array}{c}
\ldots 111^{r-1}11^{r-1}01^{r-1}11^{r-1}11\ldots \\
\ldots 111^{r-1}01^{r-1}01^{r-1}01^{r-1}11\ldots \\
\ldots 101^{r-1}01^{r-1}01^{r-1}01^{r-1}01\ldots \\
\vdots \\
\ldots 101^{r-1}01^{r-1}01^{r-1}01^{r-1}01\ldots
\end{array}$$

Figure 11: Typical orbit of $\pi_{r,0,r}(x)_i \equiv x_{i-r}x_ix_{i+r} \pmod 2$.

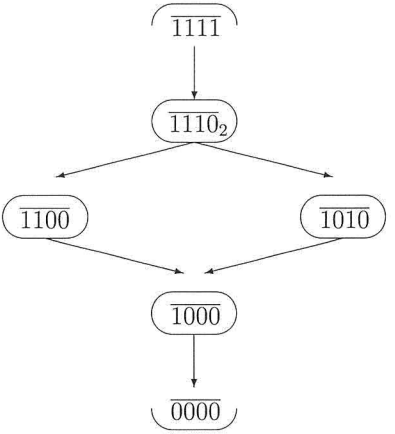

Figure 12: Phase portrait for $\pi_{4,0,4}(x)_i \equiv x_{i-4}x_ix_{i+4} \pmod 2$.

1. *There are at most* 2^r *fixed points, each given by a distinct pattern of the form* $\overline{b_1b_2\ldots b_r}$. *Each is a saddle point, except the repellor* $\overline{1}$ *and the attractor* $\overline{0}$.
2. *The basin of attraction of* $\overline{0}$ *properly contains the set of configurations with at least one block of* 0^r.

The phase portrait is similar to that in Figure 10. We give the portrait for $r = 4$ in Figure 12.

3.2 Asymmetric monomials of degree three

Consider the asymmetric monomial of degree 3 given by

$$\begin{aligned}
\pi_{r,0,k}(x)_i &\equiv x_{i-r}x_ix_{i+k} \pmod 2 \\
&\equiv \sigma^j(x_{i-(r+j)}x_{i-j}x_{i+(k-j)}) \pmod 2 \\
&\equiv \sigma^j(\pi_{r+j,j,k-j}(x))_i \pmod 2
\end{aligned}$$

We will first consider the *centered* asymmetric case and then shift it to obtain the *off-center* asymmetric case. Figure 13 illustrates the idea of *fold-*

$$\begin{array}{c}
\ldots 1111^{r-k-1}11^{r-1}11^{r-k-1}\underline{0}1^{k-1}11^{r-k-1}111\ldots \\
\ldots 1111^{r-k-1}01^{k-1}11^{r-k-1}\underline{0}1^{k-1}01^{r-k-1}111\ldots \\
\ldots 1111^{r-k-1}01^{k-1}01^{r-k-1}\underline{0}1^{k-1}01^{r-k-1}111\ldots \\
\vdots \\
\ldots 01^{r-k-1}01^{r-k-1}01^{r-k-1}\underline{0}1^{r-k-1}01^{r-k-1}\ldots
\end{array}$$

Figure 13: Folding under $\pi_{r,0,k}(x)_i \equiv x_{i-r}x_ix_{i+k} \pmod 2$.

ing. The dynamics essentially *folds* the block $01^{k-1}\underline{0}1^{r-1}0$ about the center 0, from which the limit pattern $\overline{01^{r-k-1}}$ inevitably follows.

So there are at most 2^{r-k} distinct patterns representing 2^{r-k} distinct limit cycles. Again, we summarize these observations in the following

Proposition 3.2. (The dynamics of $\pi_{r,0,k} \equiv x_{i-r}x_ix_{i+k} \pmod 2$.)
If $\hat{r} = r - k$, then

1. *There are at most $2^{\hat{r}}$ limit cycles, each given by a distinct pattern of the form $\overline{b_1b_2\ldots b_{\hat{r}}}$. Each is a saddle cycle, except for the repellor $\overline{1}$ and the attractor $\overline{0}$.*
2. *The basin of attraction of $\overline{0}$ properly contains those configurations with a block $0^{\hat{r}}$.*

Adding a shift of σ^j to the dynamics, we obtain the off-center asymmetric case. As in case of monomials of degree 2, the shift reduces the number of distinct limit cycle patterns modulo the length of the subpatterns.

Proposition 3.3. (The dynamics of $\pi_{r-j,j,k-j} \equiv x_{r-j}x_jx_{k-j} \pmod 2$.)
If $\hat{r} = r - k$, then

1. *There are at most $2^{\hat{r}}$ limit cycles, each given by a distinct pattern of the form $\overline{b_1b_2\ldots b_{\hat{r}}}$. Each is a saddle cycle, except for the repellor $\overline{1}$ and the attractor $\overline{0}$.*
2. *The basin of attraction of $\overline{0}$ properly contains those configurations with a block of $0^{\hat{r}}$.*

In keeping with the previous cases, we give an example of a phase portrait in Figure 14.

4. Higher-dimensional analogues

The two-dimensional analogue of $\pi_{r,r}(x)_i \equiv x_{i-r}x_{i+r} \pmod 2$ is a monomial of degree 4 given by

$$\pi_{r,r,r,r}(x)_i \equiv x_{i+rE}x_{i+rW}x_{i+rN}x_{i+rS} \pmod 2$$

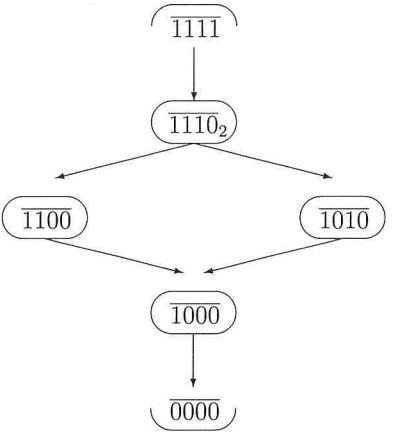

Figure 14: Phase portrait for $\pi_{4,0,8}(x)_i \equiv x_{i-4}x_ix_{i+8} \pmod 2$.

where E, W, N, and S correspond to *East*, *West*, *North*, and *South* on the von Neumann neighborhood centered at cell i

$$\begin{array}{ccc} & N & \\ W & i & E \\ & S & \end{array}$$

and rE, rW, rN, and rS denote r cells to the East of i, r cells the West of i, etc. Consider, for example, the evolution depicted in Figure 15 of the simplest perturbation of the homogenous configuration of 1s leading to a 2-cycle.

The three-dimensional analogue is easy to visualize as well and is given by

$$\pi_{r,r,r,r,r,r}(x)_i \equiv x_{i+rE}x_{i+rW}x_{i+rN}x_{i+rS}x_{i+rF}x_{i+rB} \pmod 2$$

where F and B denote the *Front* and *Back* faces of the neighborhood cube. The K-dimensional analogue has $2K$ *directions* D and global dynamics given by

$$\pi_{\underbrace{r,r,\ldots,r}_{2k}}(x)_i = \prod_{D=1}^{2K} x_{i+rD} \pmod 2.$$

The natural extension of $\pi_{r,k}$ to two dimensions is

$$\pi_{r_1,r_2,k_1,k_2}(x)_i \equiv x_{i+r_1E}x_{i+r_2W}x_{i+k_1N}x_{i+k_2S} \pmod 2$$

which has the one-sided special case

$$\begin{aligned} \pi_{r_1,0,k_1,0}(x)_i &\equiv x_{i+r_1E}x_ix_{i+k_1N}x_i \pmod 2 \\ &\equiv x_{i+r_1E}x_i^2x_{i+h_2N} \pmod 2. \end{aligned}$$

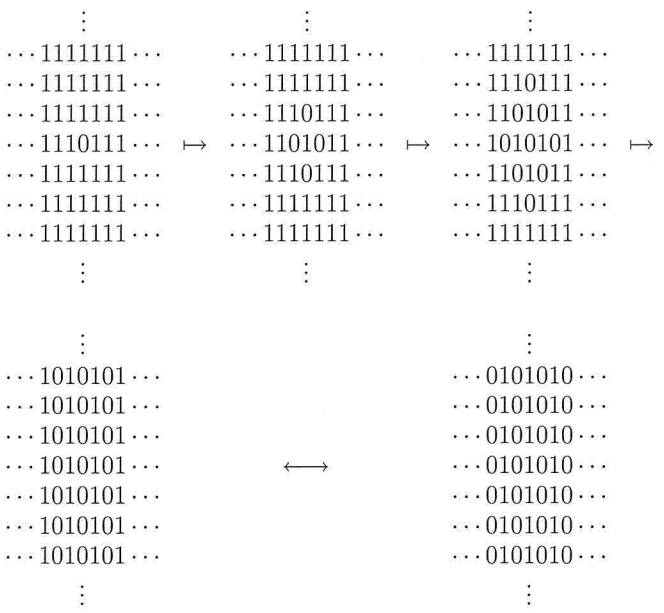

Figure 15: An orbit of $\pi_{1,1,1,1}(x)_i \equiv x_{i+E}x_{i+W}x_{i+N}x_{i+S} \pmod 2$, the two-dimensional analogue of the orbit computed earlier.

Consider the orbit for $r_1 = 3$ and $k_1 = 2$ given in Figure 16, which tends to a fixed point with the upper half-plane all 1s and right half-plane all 1s. Clearly this is the two-dimensional analogue we seek, with countably many fixed-points for each two-dimensional pattern of 0s and 1s. Higher-dimensional analogues should be equally visible to the reader. The two-sided, shifted dynamics is also easy to visualize, leaving only the details of the cycle lengths, which we omit.

The two-dimensional analogue of $\pi_{r,0,r}$ is given by

$$\pi_{r,r,0,r,r}(x)_i \equiv x_{i+rE}x_{i+rW}x_ix_{i+rN}x_{i+rS} \pmod 2.$$

In Figure 17, we give the simplest orbit for the $r = 2$ case. The strictly fixed-point dynamics is clear from the one-dimensional case, as should be the dynamics for three and higher dimensions.

The two-dimensional analogue of $\pi_{r,0,k}$ above is given by

$$\pi_{r_1,r_2,0,k_1,k_2}(x)_i \equiv x_{i+r_1E}x_{i+r_2W}x_ix_{i+k_1N}x_{i+k_2S} \pmod 2.$$

Folding occurs in both directions, but is difficult to portray in limited space, so we omit the example. However, the dynamics should be clear from the one-dimensional case, as should the dynamics for three and higher dimensions.

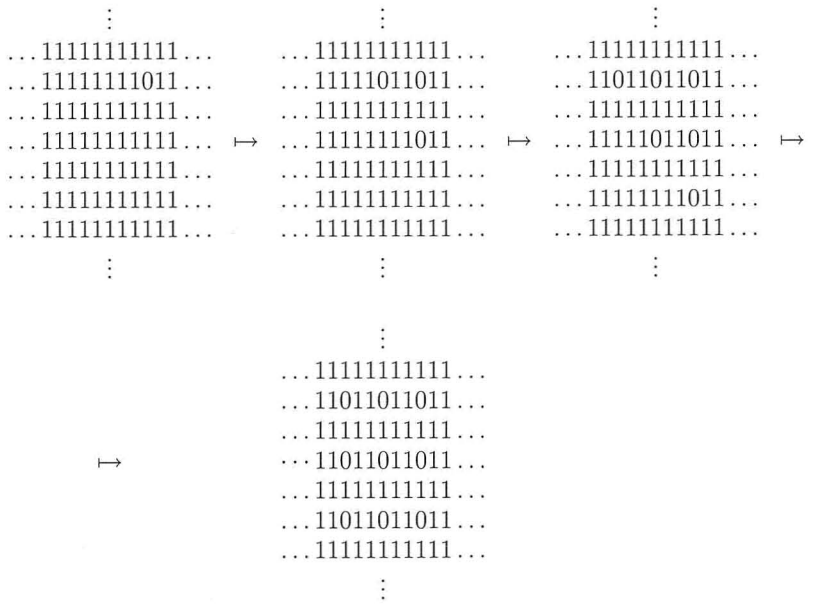

Figure 16: An orbit of $\pi_{3,0,2,0}(x)_i \equiv x_{i+3E}x_i^2x_{i+2N} \pmod 2$.

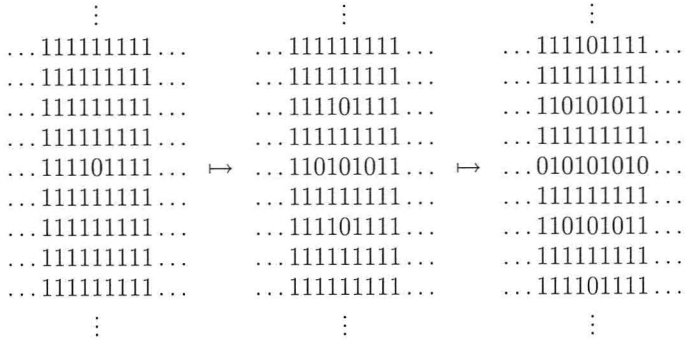

Figure 17: An orbit of $\pi_{2,2,0,2,2}(x)_i \equiv x_{i+2E}x_{i+2W}x_ix_{i+2N}x_{i+2S} \pmod 2$, the two-dimensional analogue of the orbit computed with $r = 2$.

The two-dimensional analogue of the shifted version of the above requires combining two shifts, one for each dimension.

$$\pi_{r_1-j,r_2-j,j,l,k_1-l,k_2-l}(x)_i \equiv x_{i+(r_1-j)E}x_{i+(r_2-j)W}x_{i+jE+lN}x_{i+(k_1-l)N}x_{i+(k_2-l)S} \pmod 2.$$

For example, if the North-South shift is $2N$ and the East-West shift is $3E$, then the resultant shift is $2N + 3E$. Other than this, the dynamics follows the one-dimensional case. Similarly, three components are used to compute the resultant shift in the 3D case.

An interesting monomial of degree two in two dimensions

While searching for two-dimensional analogues of monomials of degree 2, we discovered an interesting case given by

$$\pi(x)_i \equiv x_{i+E}x_{i+N} \pmod 2.$$

Initially, this seemed analogous to the one-sided dynamics of $\pi_{0,r}(x)_i \equiv x_i x_{i+r}$ (mod 2). However, this is a monomial of degree 2 in two dimensions, hence it is an analogue in a different sense than the degree-4 monomials above. In this case, all finite perturbations of $|\underline{1}|$ (the homogenous configuration of 1) by 0s disappear to the South-West. A verticle line of 0s perturbing a sea of 1s reproduces itself downward and to the left (NE idemprop), eventually tending to the configuration with a half-plane of 0s to the left of the line and a half-plane of 1s to the right. We denote this configuration by $0|1$. Similarly, a horizontal line of 0s tends to $\frac{1}{0}$, the configuration with a half-plane of 1s above the line and a half-plane of 0s below. Interestingly, lines of 0s with positive, rational slope m/n tend to cycles with period $m+n$, while lines of 0s with negative, rational slope disappear to the South-West, tending to $|\underline{1}|$. All this is also true for half-lines.

Essentially, the rule propagates parallel lines of 0s with slope -1 corresponding to the NE idemprop. Each cell eventually cycles with period $m+n > 1$ if and only if there is a half-line of 0s with slope $0 < m/n < \infty$. In that case, there are eventually periodic points of every period. We give an example in Figure 18 where $m = n = 1$ tends toward a 2-cycle.

We extend this map to asymmetric neighborhoods in a natural way, namely,

$$\pi_{r,k}(x)_i \equiv x_{i+rE}x_{i+kN} \pmod 2.$$

This map propagates parallel lines of 0s with slope $-k/r$ corresponding to the $kNrE$ idemprop. As in the case $r = 1 = k$ above, finite perturbations of $|\underline{1}|$ by 0s disappear to the South-West. Infinite perturbations by lines of 0s with negative slope also disappear to the South-West. A vertical line of 0s is copied r places to the West, while a horizontal line of 0s is copied k places to the South. Again, lines of 0s with positive slope tend to limit cycles. A line with slope m/n for $m, n \in \mathbf{Z}^+$ tends to a cycle of length $\mathrm{lcm}(k,m)+\mathrm{lcm}(r,n)$, where $\mathrm{lcm}(x,y)$ is the *least common multiple* of x and y.

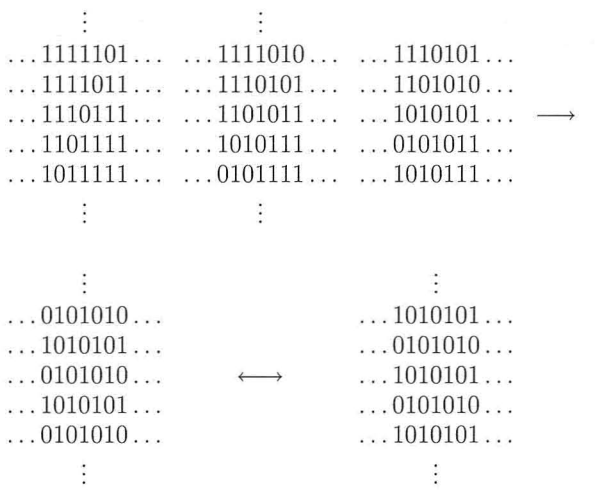

Figure 18: A limit cycle in $\pi(x)_i \equiv x_{i+N}x_{i+E} \pmod 2$.

Other neighborhoods—such as the Moore neighborhood or the Margolis neighborhood, as well as more general grids—have similar features and can be analyzed using the same techniques.

5. Extended state sets

Next we consider the effects of introducing more states. Reimen [4] has shown that a CA over a commutative monoid has divergent orbits with space-time trajectories isomorphic to Pascal's triangle modulo m. For m with primitive roots, this can also be inferred for the cyclic groups $\langle \mathbf{Z}_m, \bullet \rangle$ from the work on linear CAs over $\langle \mathbf{Z}_m, + \rangle$ by Aso and Honda [2] using the topological conjugacy provided by the discrete logarithm (2), except for the additional 0. Here we show that there may also be more limit cycles.

Consider the monomial in one dimension given by

$$\pi_{1,1}(x)_i \equiv x_{i-1}x_{i+1} \pmod{14}$$

and the orbit of $x = \overline{5}$ with $H = 11$ below.

...5555555...
...9999999...
...*HHHHHHH*...
...9999999...
...*HHHHHHH*...

In the example above, $\overline{5}$ has idempotent degree 2 and idempotent order 2.

Now consider the homogenous configuration $\overline{s}$. Clearly, if $s^2 = s$, then $x_{i-r}x_{i+r} = s$, for every i (and r), and $\overline{s}$ is a fixed point. Now if $s^4 = s$, but $s^2 \neq s$, then $\overline{s}$ is a 2-cycle. Continuing, if $s^{2t} = s$, but $s^{2t'} \neq s$ for $t' < t$, then $\overline{s}$ is a t-cycle. In the example above, $s = 4$, $s^2 = 2$, and we have a one-step transient, which we might refer to as $\sqrt{s} = 8$. The phase portrait for $x_{i-1}x_{i+1} \pmod{10}$ is the same as that for $x_{i-1}x_{i+1} \pmod{6}$ given in Figure 12.

More examples

The monomial $\pi_{1,1}(x)_i \equiv x_{i-1}x_{i+1} \pmod{3}$ over $\langle \mathbf{Z}_3^*, \bullet \rangle$ has been extensively analyzed under the guise of its isomophic image, the additive CA with local rule $\delta(x)_i \equiv x_{i-1} + x_{i+1} \pmod{2}$ (see Wolfram Rule 90). By including 0, we obtain the state set $\langle \mathbf{Z}_3, \bullet \rangle$. We already know the general dynamics on configurations consisting only of 0s and 1s. From previous work on Rule 90, we obtain the dynamics on $\{1, 2\}$-configurations. And since $2^2 \equiv 1 \pmod{3}$, we also know the dynamics for $\{0, 2\}$-configurations, as illustrated below.

$$\ldots 222222\underline{0}2222222 \ldots$$
$$\ldots 111111\underline{0}1111111 \ldots$$

Only the $\{0, 1, 2\}$-configurations remain, which have the divergent dynamics of the space-time trajectories of Pascal's triangle modulo m, as seen in the following orbit.

$$\ldots 111111\underline{0}2111111 \ldots$$
$$\ldots 111112\underline{0}10211111 \ldots$$
$$\ldots 111120\underline{2}0021111 \ldots$$
$$\ldots 111201\underline{0}10102111 \ldots$$
$$\ldots 112020\underline{1}1020211 \ldots$$
$$\ldots 120102\underline{0}10201021 \ldots$$
$$\vdots$$

The phase portrait is given in Figure 19.

The phase portrait for $\pi_{1,1}(x)_i \equiv x_{i-1}x_{i+1} \pmod{4}$ is similar to that for $\pi_{1,1}(x)_i \equiv x_{i-1}x_{i+1} \pmod{2}$ given in Figure 5. No new limit cycles are added; only divergent orbits appear. The phase portrait for $\pi_{1,1}(x)_i \equiv x_{i-1}x_{i+1} \pmod{5}$ is similarly repetitive.

Figure 20 gives the phase portrait for $\pi_{1,1}(x)_i \equiv x_{i-1}x_{i+1} \pmod{6}$. The phase portrait for $\pi_{1,1}(x)_i \equiv x_{i-1}x_{i+1} \pmod{10}$ is the same as that in Figure 20, provided $3 \to 5$ and $4 \to 6$. Again not all arrows are present. An exception here is that not every pattern lower in the digram can be reached from a pattern above it. However, every limit cycle pattern can be reached via a perturbation of $\overline{1}$. In addition to the limit cycles, there are divergent orbits with space-time trajectories of Pascal's triangle modulo m. See, for example, Figure 21 (where (*) is either 2 or 5, initially 5).

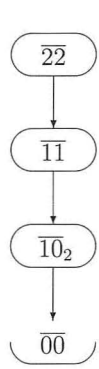

Figure 19: Phase portrait for $\pi_{1,1}(x)_i \equiv x_{i-1}x_{i+1} \pmod 3$.

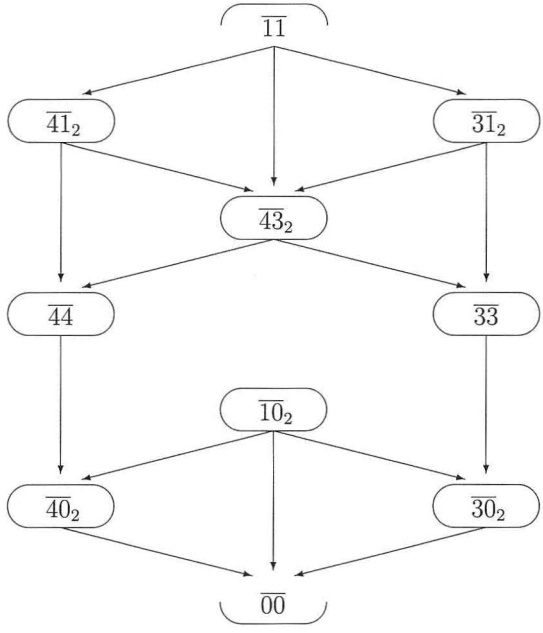

Figure 20: Phase portrait for $\pi_{1,1}(x)_i \equiv x_{i-1}x_{i+1} \pmod 6$.

```
11111111111111111111**11111111111111111111
11111111111111111111****11111111111111111111
11111111111111111111**41**11111111111111111111
11111111111111111111********11111111111111111111
11111111111111111111**414141**11111111111111111111
11111111111111111111****4141****11111111111111111111
11111111111111111111**41**41**41**11111111111111111111
11111111111111111111**********11111111111111111111
11111111111111**41414141414141**11111111111111
11111111111111****414141414141****11111111111111
11111111111111**41**4141414141**41**11111111111111
11111111111111********41414141********11111111111111
11111111111**414141**414141**414141**11111111111
11111111111****4141****4141****4141****1111111111
11111111**41**41**41**41**41**41**41**11111111
11111111**********************************11111111
```

Figure 21: A divergent orbit of $\pi_{1,1}(x)_i \equiv x_{i-1}x_{i+1} \pmod 4$.

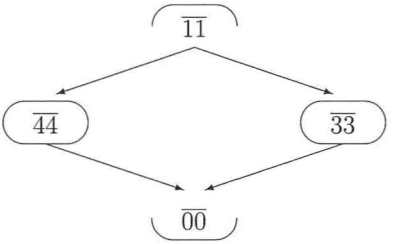

Figure 22: Phase portrait for $\pi_{2,0,1}(x)_i \equiv x_{i-2}x_ix_{i+1} \pmod 6$.

Clearly, these monomials fall into Wolfram Class II since every limit cycle can be determined in finite time from one of a finite number of perturbations of $\overline{s}$, for some $s \in \mathbf{Z_m}$.

As a final example, we present in Figure 22 the phase portrait for $\pi_{2,0,1}(x)_i \equiv x_{i-2}x_ix_{i+1} \pmod 6$.

6. Conclusion

Monomials of arbitrary degree can be obtained as a product of monomials of degrees 2 and 3. Monomials of even degree are the product of monomials of degree 2. Monomials of odd degree greater than 3 are the product of a monomial of degree 3 and monomials of even degree. We apply the superposition principle to find the limit cycles. Given an initial configuration, limiting

configurations are the pointwise multiplication modulo m of the respective limiting configurations under the component monomials of degrees 2 and 3.

Monomial CAs over $\langle \mathbf{Z}_m, \bullet \rangle$ fall into the first three Wolfram Classes. We need only simulate the dynamics over a finite window for a finite time to determine whether they obtain a particular orbit.

Acknowledgments

The work of the first author was partially funded through the Institute for Intelligent Systems at The University of Memphis.

References

[1] M. Ito, N. Osato, and M. Nasu, "Linear Cellular Automata over $\mathbf{Z_m}$," *Journal of Computer and System Sciences*, **27** (1983) 125–140.

[2] H. Aso and N. Honda, "Dynamical Characteristics of Linear Cellular Automata," *Journal of Computer and System Sciences*, **30** (1985) 291–317.

[3] T. Sato, "Decidability for Some Problems of Linear Cellular Automata over Finite Commutative Rings," *Information Processing Letters*, **46** (1993) 151–155.

[4] N. Reimen, "Superposable Treillis Automata," *Proceedings of MFCS '91*, LNCS, (1991) 13–24. Also PhD Thesis, École Normale Supérieure de Lyon (1992).

[5] G. A. Hedlund, "Endomorphisms and Automorphisms of the Shift Dynamical System," *Mathematical Systems Theory*, **3** (1969) 320–375.

[6] C. T. Long, "Pascal's Triangle Modulo p," *Fibonacci Quarterly*, **19** (1981) 458–463.

[7] B. Voorhees, "Cellular Automata, Pascal's Triangle, and Generation of Order," *Physica D*, **31** (1988) 135–140.

[8] S. Wolfram, "Geometry of Binomial Coefficients," *American Mathematical Monthly*, (1984) 566–571.

[9] W. J. LeVeque, *Topics in Number Theory, Vol. 1* (Reading, MA: Addison-Wesley, 1956).

[10] K. Culik II and S. Yu, "Undecidability of CA Classification Schemes," *Complex Systems*, **2** (1988) 177–190.

[11] S. Wolfram, "Universality and Complexity in Cellular Automata," *Physica D*, **10** (1984) 1–35. Reprinted in S. Wolfram, editor, *Theory and Applications of Cellular Automata* (Singapore: World Scientific, 1987).